Hue University Journal of Science: Natural Science
Vol. 134, No. 1S-1, 5–14, 2025

pISSN 1859-1388
eISSN 2615-9678

Green synthesis of nickel ferrite nanoparticles using starch for visible-light photocatalytic degradation of crystal violet

Do Mai Nguyen[1], Vo Chau Ngoc Anh[1,2]*

[1] University of Sciences, Hue University, 77 Nguyen Hue St., Hue, Vietnam
[2] University of Medicine and Pharmacy, Hue University, 6 Ngo Quyen St., Hue, Vietnam

* Correspondence to Vo Chau Ngoc Anh <vcnanh@hueuni.edu.vn>

(*Received: 07 May 2025; Revised: 05 June 2025; Accepted: 19 June 2025*)

Abstract. This study presents the green synthesis of $NiFe_2O_4$ nanoparticles with starch as a reducing and stabilising agent. The material was characterised with XRD, FT-IR, SEM, TEM, BET, and UV–Vis DRS, confirming a spinel structure, mesoporosity (58.3 m^2/g), uniform spherical morphology (10–20 nm), and a band gap of 2.54 eV. Photocatalytic degradation of crystal violet under visible light achieved a 76.0% efficiency within 120 minutes, following pseudo-first-order kinetics. Compared with other photocatalysts, $NiFe_2O_4$ exhibits superior activity. The starch-mediated green synthesis improved dispersion and photocatalytic performance, offering a sustainable route for efficient visible-light-driven photocatalysts in environmental remediation.

Keywords: $NiFe_2O_4$, photocatalysis, crystal violet, degradation, visible light

1 Introduction

The increasing contamination of water sources due to the discharge of industrial effluents, particularly from textile, food, and paper industries, has raised significant concerns regarding environmental and human health risks [1–3]. Among the most prevalent contaminants are synthetic dyes, especially crystal violet (CV), which are widely used in various industrial applications. These dyes are known for their stability and persistence in the environment and toxicity, making their removal from wastewater an urgent environmental challenge [4]. Traditional methods for dye removal, such as adsorption and coagulation, often lack efficiency and are not suitable for large-scale applications. Therefore, advanced techniques, particularly photocatalysis, have gained attention because of their capacity to degrade organic pollutants under light irradiation [5, 6].

Photocatalysis has proven to be an effective and sustainable approach for the degradation of organic contaminants in wastewater. Metal oxide semiconductors, such as TiO_2, ZnO, and $NiFe_2O_4$, have been extensively studied because of their capacity to generate reactive oxygen species (ROS) under light irradiation, which can break down organic pollutants into non-toxic by-products [7, 8]. Among these materials, $NiFe_2O_4$ emerged as a promising photocatalyst because of its unique properties, such as a narrow bandgap (2.0 to 2.5 eV), high stability, and magnetic properties that allow for easy recovery from solutions [9, 10]. Moreover, $NiFe_2O_4$'s capacity to absorb visible light makes it particularly attractive for photocatalytic applications, as it can be activated by sunlight, which is a readily available and renewable energy source [11–13].

The photocatalytic activity of $NiFe_2O_4$ can be significantly influenced by its synthesis method, particle size, and surface area. Materials

with mesoporous structures have been shown to exhibit enhanced photocatalytic performance because of the increased number of active sites available for adsorption and reaction [5, 9]. In particular, $NiFe_2O_4$ nanoparticles with a large surface area have been reported to demonstrate excellent photocatalytic degradation of various organic dyes, including CV, under visible light. Additionally, the use of green synthesis methods, such as utilising renewable resources like starch as a reducing agent, aligns with the growing demand for eco-friendly and sustainable production techniques [14–16].

Recent research has also focused on improving the photocatalytic efficiency of $NiFe_2O_4$ by modifying its morphology and crystallinity. Studies have shown that calcination at various temperatures can alter the crystallite size and surface properties of $NiFe_2O_4$, affecting its photocatalytic efficiency. The synthesis of $NiFe_2O_4$ with starch has been reported to result in nanoparticles with favourable properties for photocatalysis, including high dispersion, smaller particle sizes, and larger surface areas [13, 17].

This study aims to synthesise $NiFe_2O_4$ nanoparticles with a green approach with starch and evaluate their photocatalytic activity for the degradation of CV under visible light. The synthesis, characterisation, and photocatalytic performance of $NiFe_2O_4$ will be compared with that of other commonly used photocatalysts, highlighting its potential for environmental applications in wastewater treatment.

2 Experimental

2.1 Chemical

The chemicals used in this study include $Ni(NO_3)_2{\cdot}6H_2O$ (99.99%), $Fe(NO_3)_3{\cdot}9H_2O$ (99.99%), starch (≥99%, China), and crystal violet (≥99%, Merck, Germany).

2.2 Instrument

The equipment used in this study includes an ultrasonic machine, an oven, a furnace, a Precisa XB 220 analytical balance (Switzerland), a magnetic stirrer, a centrifuge, and an Osram lamp (160 W, 240 V).

The crystal phase composition of the material was determined by using X-ray diffraction (XRD) on a Bruker D8-Advance diffractometer (Germany), with a Cu anode X-ray tube, λ(Cu-Kα) = 1.540 Å, 30 kV, 0.01 A, scan step of 0.1°/s, and scan angle range of 10–60°. The morphology, structure, and relative size of the material were observed by using transmission electron microscopy (TEM) on a JEOL JEM-1010 instrument (Japan). The surface morphology of the photocatalyst was observed on a field emission scanning electron microscope (FESEM, Hitachi S-4800, Japan). The specific surface area (BET) of the material was determined by using N_2 adsorption-desorption at 77 K on a Micromeritics TriStar II Plus 3030 apparatus (USA). The band gap energy of the material was determined by using ultraviolet-visible diffuse reflectance spectroscopy (UV-Vis DRS) recorded on a $BaSO_4$ substrate using a UV2600 spectrophotometer (Shimadzu, Japan). UV-Vis spectra were recorded with a UViline 9400 and an Analytik Jena AG - SPECORD 50 UV-VIS spectrophotometer with a quartz cuvette.

2.3 Synthesis of nickel ferrite

$Ni(NO_3)_2{\cdot}6H_2O$, $Fe(NO_3)_3{\cdot}9H_2O$, starch (PA, China), and H_2O were mixed in a 100 mL round-bottom flask at a Ni^{2+}/Fe^{3+} ratio of 2.0, a molar ratio of starch/(Ni^{2+} + Fe^{3+}) of 1.5, and a molar ratio of H_2O/starch of 120. The reaction mixture was stirred and heated to 80 °C for one hour to dissolve the starch. Subsequently, the entire mixture was transferred into a hydrothermal reactor and treated at 180 °C for 24 hours. The product was washed several times with distilled

pISSN 1859-1388
eISSN 2615-9678

water, then dried at 100 °C until a constant weight was achieved, resulting in $NiFe_2O_4$. The sample obtained after the hydrothermal treatment was calcined at 700 °C for three hours to promote the crystallisation of the material, designated as $NiFe_2O_4$-700 [9, 18, 19].

2.4 Photocatalytic activity investigation

The photocatalytic reactor was composed of a 250 mL Erlenmeyer flask, which was positioned on a magnetic stirrer inside a wooden chamber with dimensions of 24 × 40 × 40 cm. A tungsten filament lamp (Osram, 160 W, Germany) was employed as a simulated sunlight source and was fixed at a distance of 7 cm above the reaction vessel. An opening was incorporated at the top of the chamber to allow light irradiation, while a ventilation fan was installed on the side to maintain a stable reaction temperature of approximately 27 °C. For each photocatalytic experiment, 100 mL of CV solution at various initial concentrations (10, 15, 20, and 25 ppm) was introduced into the flask, followed by the addition of 0.05 g of the synthesised $NiFe_2O_4$ photocatalyst. Prior to exposure to light, the suspension was stirred in the dark for 60 minutes to establish adsorption-desorption equilibrium. Throughout both the dark and irradiation phases, 5 mL aliquots of the reaction mixture were withdrawn at predetermined intervals and subjected to centrifugation for catalyst separation. The concentration of CV in the obtained supernatant was subsequently determined UV-Vis spectroscopically at a wavelength of 585 nm.

The photocatalytic degradation efficiency of CV was calculated with the following formula

$$F\ (\%) = \frac{(C_0 - C_t) \times 100}{C_0}$$

where C_0 and C_t represent the initial concentration of CV and the concentration of CV at time t.

3 Results and discussion

3.1 Characterisation of spinel nickel ferrite

The X-ray diffraction (XRD) patterns of both uncalcined $NiFe_2O_4$ and $NiFe_2O_4$-700 (calcined at 700 °C) exhibit characteristic peaks at 18.6, 30.3, 35.7, 37.2, 43.4, 54.1, and 57.4°, corresponding to the (111), (220), (311), (222), (400), (422), and (511) planes (JCPDS Card No. 10-0325), indicative of the spinel cubic structure (Figure 1) [11, 14]. The crystallite size of the uncalcined $NiFe_2O_4$ is 12.3 nm, while the calcined $NiFe_2O_4$-700 exhibits a larger crystallite size of 18.9 nm. The broader and less intense diffraction peaks of the uncalcined material suggest a more amorphous structure. These findings are consistent with those from recent studies, reporting similar XRD patterns and crystallite sizes for $NiFe_2O_4$ nanoparticles [12, 17]. $NiFe_2O_4$ underwent further analysis because of its favourable structure, well-suited for the subsequent photocatalytic studies [20].

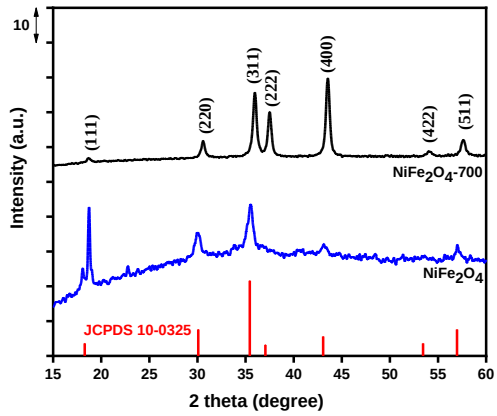

Fig. 1. XRD pattern of $NiFe_2O_4$

The FT-IR spectrum of $NiFe_2O_4$ exhibits characteristic peaks at 3381, 2987, 1610, 1392, 1319, and 590 cm^{-1} (Figure 2). These bands are consistent with the typical vibrational modes of $NiFe_2O_4$, including the stretching vibration of O–H groups at 3381 cm^{-1}, the stretching vibration of C–H bonds at 2987 cm^{-1}, and the Fe–O stretching modes at 590 cm^{-1}. The observed peaks align with those reported in recent studies,

supporting the identification of the material as $NiFe_2O_4$ [21, 22].

The nitrogen adsorption/desorption isotherms of $NiFe_2O_4$ reveal a type IV isotherm with a hysteresis loop, characteristic of mesoporous materials (Figure 3). The specific surface area (S_{BET}) of the $NiFe_2O_4$ material was calculated to be 58.3 m^2/g. These results indicate that the material possesses a significant surface area, which is consistent with the findings in recent studies on $NiFe_2O_4$ nanoparticles, where similar nitrogen adsorption behaviour and surface areas were observed. These findings are in agreement with those in recent publications, which reported similar surface areas and mesoporous structures for $NiFe_2O_4$, further confirming its potential as a suitable material for photocatalytic applications [19, 23, 24].

The scanning electron microscopy (SEM) image of $NiFe_2O_4$ shows well-dispersed nanoparticles with a relatively uniform size distribution (Figure 4). The morphology observed suggests the presence of spherical particles, which is consistent with recent studies on $NiFe_2O_4$ nanoparticles. This structural characteristic is often associated with improved photocatalytic activity because of enhanced surface area and active site availability. These results are in agreement with similar findings in the literature, where $NiFe_2O_4$ nanoparticles with spherical morphology have been reported for photocatalytic applications [9, 10, 18].

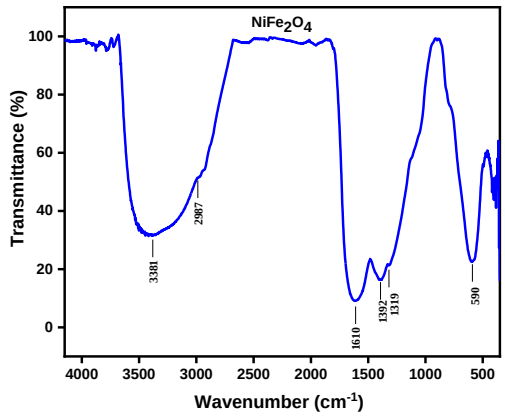

Fig. 2. FT-IR spectrum of $NiFe_2O_4$

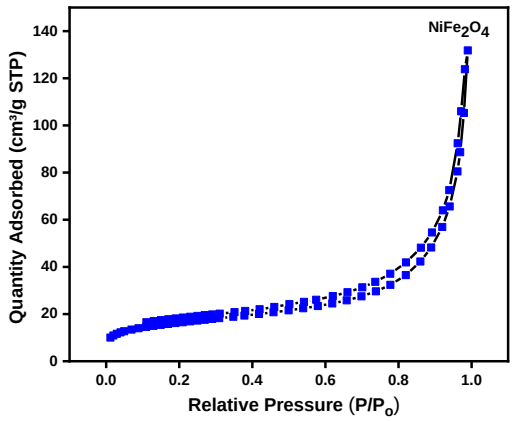

Fig. 3. Nitrogen adsorption/desorption isotherms of $NiFe_2O_4$

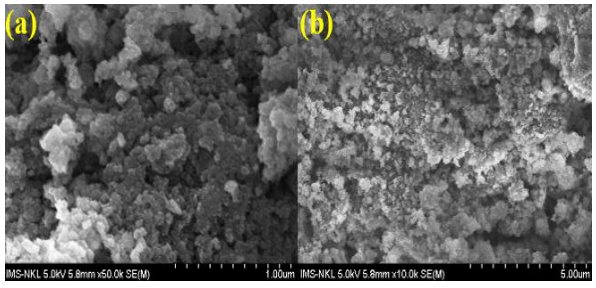

Fig. 4. SEM image of $NiFe_2O_4$

The transmission electron microscopy (TEM) analysis of $NiFe_2O_4$ reveals the nanoparticles' size and confirms the uniform distribution of particles, with an average size in the range of 10–20 nm (Figure 5). This observation supports the crystallite size obtained from XRD analysis. The TEM results align with recent

pISSN 1859-1388
eISSN 2615-9678

reports on $NiFe_2O_4$, indicating that the nanoparticles are of appropriate size for photocatalytic processes, where small particle size is often advantageous for increased reactivity. The results are consistent with those in recent studies on $NiFe_2O_4$ nanoparticles for photocatalytic degradation [14, 24, 25].

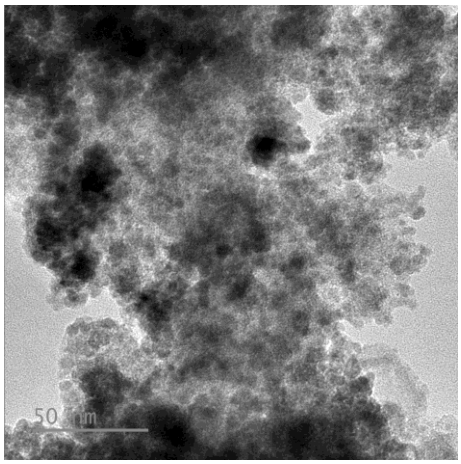

Fig. 5. TEM image of $NiFe_2O_4$

The UV-Vis diffuse reflectance spectrum of $NiFe_2O_4$ was recorded and analysed to elucidate its optical absorption characteristics, which are critical for its photocatalytic behaviour. As shown in Figure 6, a distinct absorption edge was observed in the visible light region, confirming the material's capability to harvest visible photons. This absorption onset was attributed to the electronic transitions associated with the intrinsic band structure of $NiFe_2O_4$ [16, 23].

The band gap energy (E_g) was estimated by applying the Tauc plot method to the UV-Vis data, where the $(\alpha h\nu)^2$ values versus photon energy ($h\nu$) was plotted, assuming a direct allowed transition. From the extrapolation of the linear portion of the Tauc plot, the band gap was determined to be approximately 2.54 eV. This value is consistent with previously reported band gaps for $NiFe_2O_4$ nanoparticles synthesised via similar routes [16, 23].

Such a band gap enables effective excitation under visible light irradiation, promoting the generation of electron-hole pairs, essential for photocatalytic activity. The absorption in the visible region is mainly governed by the d-d transitions of the Ni^{2+} and Fe^{3+} ions in the spinel lattice and charge transfer between metal ions and oxygen ligands [16, 23].

Furthermore, the significant light absorption capacity within the visible range explains the high photocatalytic degradation efficiency observed for CV under simulated sunlight. The broad absorption spectrum ensures that a substantial fraction of incident photons can be utilised for reactive oxygen species generation, thereby enhancing the degradation rates [16, 23].

Therefore, the UV-Vis spectrum presented in Figure 6 substantiates the suitability of $NiFe_2O_4$ as a visible-light-driven photocatalyst. The experimentally obtained band gap supports the material's capacity to harness visible-light energy, which correlates directly with its demonstrated photocatalytic performance [16, 23].

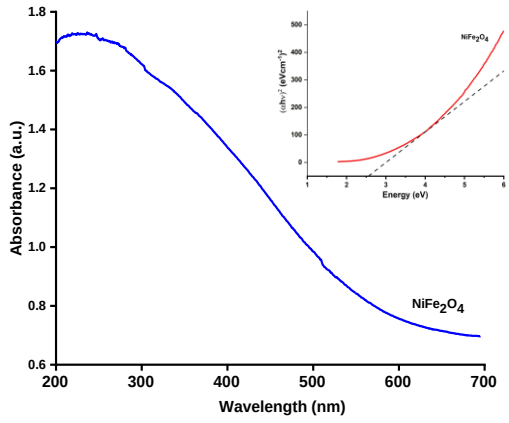

Fig. 6. UV-Vis DRS spectra and Tauc plot of $NiFe_2O_4$

The energy-dispersive X-ray (EDX) spectrum of $NiFe_2O_4$ confirms the presence of the nickel (Ni) and iron (Fe) elements, with a Ni/Fe ratio of approximately 2:1 (Figure 7). The element distribution images show a uniform distribution of Ni and Fe in the sample, supporting the

homogeneous composition of the material. These results are consistent with the expected composition of $NiFe_2O_4$ and are in agreement with those of recent studies, reporting similar elemental distribution and compositions in $NiFe_2O_4$ nanoparticles. These findings align with the results from recent studies on $NiFe_2O_4$, where similar elemental distributions and ratios were observed [9, 18, 19].

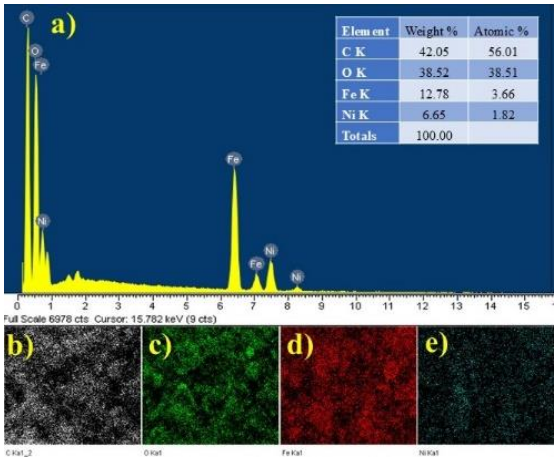

Fig. 7. (a) EDX spectra and (b-e) element distribution of $NiFe_2O_4$

The graph shows the photocatalytic degradation of CV under visible light, where $NiFe_2O_4$ exhibits significant dye degradation compared with the blank sample (Figure 8). The data were obtained by monitoring the ratio of the concentration of CV (C/C_0) over time.

During the first 60 minutes, a dark adsorption phase was observed for both $NiFe_2O_4$ and the blank sample, where no significant change in the CV concentration occurred. However, once the light irradiation began (after 60 minutes), the photocatalytic degradation of CV on $NiFe_2O_4$ was activated, resulting in a significant decrease in the concentration of CV. After 120 minutes of light exposure, a degradation efficiency of 76.0% was obtained, whereas the blank sample exhibited negligible degradation, with an efficiency of 20.1%. This behaviour is consistent with that in recent studies, which have also reported a significant photocatalytic degradation performance of $NiFe_2O_4$ under visible light. The results highlight the effective photocatalytic properties of $NiFe_2O_4$, which are in agreement with those in previous works where similar photocatalysts demonstrated high efficiencies for dye degradation under visible light.

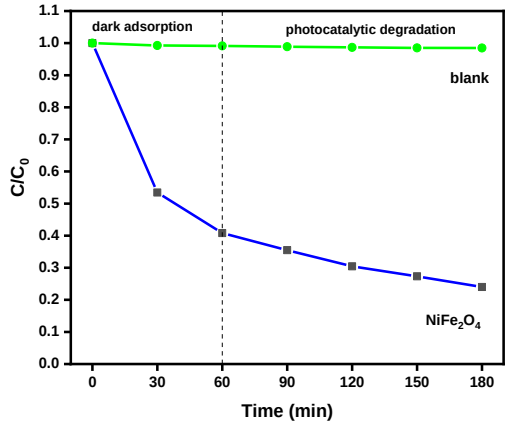

Fig. 8. Photocatalytic degradation activity of CV on $NiFe_2O_4$ and blank sample over time ($V_{solution}$ = 100 mL; $C_{0(CV)}$ = 10 ppm; $m_{material}$ = 0,05 g; t_{dark} = 60 min; t_{light} = 120 min, λ_{max} = 585 nm).

The UV-Vis spectra of CV and the treated solution after photocatalytic degradation show a significant decrease in the absorption peak of CV at 585 nm, indicating the successful degradation of the dye (Figure 9). This observation is consistent with the photocatalytic results, where $NiFe_2O_4$ effectively degrades CV under visible light. The decrease in absorbance is in line with the results obtained in similar studies, confirming the effectiveness of $NiFe_2O_4$ for dye degradation. These findings are supported by similar studies in the literature, where the photocatalytic degradation of CV using $NiFe_2O_4$ was confirmed by UV-Vis spectral analysis [16, 20].

pISSN 1859-1388
eISSN 2615-9678

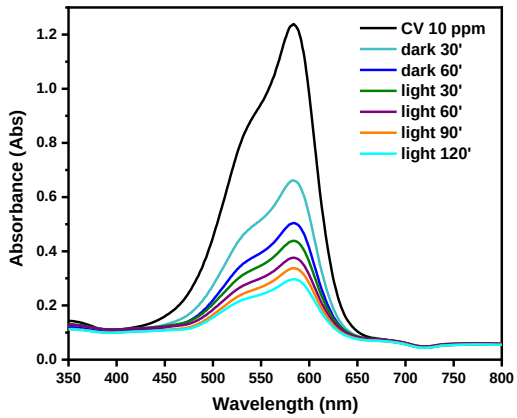

Fig. 9. UV-Vis spectra of CV and treated solution ($V_{solution}$ = 100 mL; $C_{0(CV)}$ = 10 ppm; $m_{material}$ = 0,05 g; t_{dark} = 60 min; t_{light} = 120 min, λ_{max} = 585 nm).

3.2 Photocatalytic degradation activity of the synthesised material

In Figure 10a, the kinetics of CV degradation on $NiFe_2O_4$ at different initial concentrations (10, 15, 20, and 25 ppm) are presented. The data clearly show that as the initial concentration of CV increases, the degradation rate decreases. The CV concentration decreases with time under visible-light irradiation, with the most significant reduction observed at the lowest initial concentration (10 ppm). After 120 minutes, the CV concentration for the 10 ppm sample decreased by 76.0%, as indicated in Table 1, while the degradation at higher concentrations, such as 25 ppm, was less efficient. This trend is consistent with the expected behaviour for photocatalytic processes, where lower concentrations typically result in higher degradation rates because of the higher availability of active sites for adsorption and reaction.

In Figure 10b, the natural logarithm of the concentration ratio ($\ln(C_t/C_0)$) is plotted against time for each initial concentration, showing the characteristic linear relationship expected for a pseudo-first-order reaction. The slopes of the lines correspond to the rate constant (k_{app}), and the R^2 values confirm a good fit for the first-order kinetic model. The calculated rate constants (k_{app}) for each concentration (10, 15, 20, and 25 ppm) are 4.5 × 10^{-3}; 1.3 × 10^{-3}; 1.2 × 10^{-3} and 0.5 × 10^{-3} min^{-1}, respectively, with the R^2 values ranging from 0.993 to 0.996, demonstrating excellent agreement with the first-order model.

These findings indicate that $NiFe_2O_4$ exhibits high photocatalytic activity for the degradation of the CV dye, and the efficiency decreases as the initial concentration increases. This is likely because of the saturation of available active sites and reduced penetration of light into the solution. The kinetic parameters derived from the data further support the suitability of $NiFe_2O_4$ as an efficient photocatalyst for dye degradation under visible light.

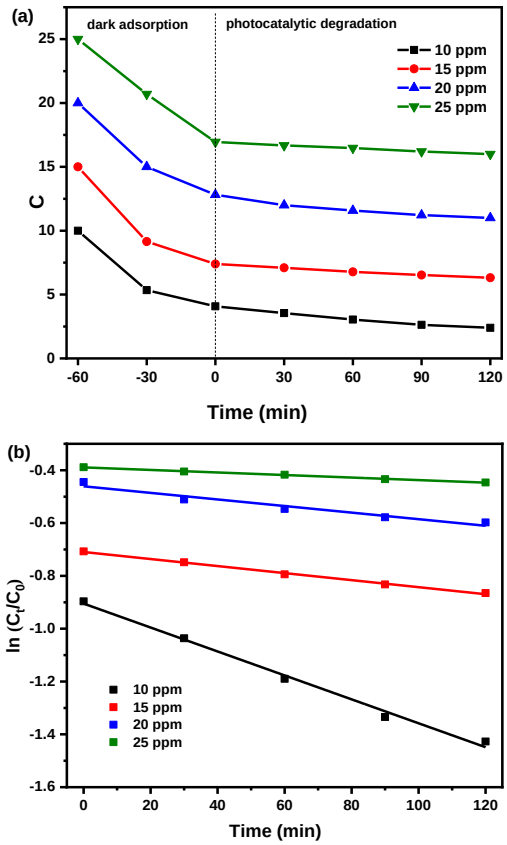

Fig. 10. (a) Kinetics of CV degradation on $NiFe_2O_4$ at several initial concentrations, (b) Plot of $\ln(C/C_0)$ vs. time. ($V_{solution}$ = 100 mL; $C_{0(CV)}$ = 10–25 ppm; $m_{material}$ = 0,05 g; t_{dark} = 60 min; t_{light} = 120 min, λ_{max} = 585 nm)

Table 1. Kinetic parameters of CV degradation on $NiFe_2O_4$ material

C (ppm)	*F*%	k_{app} (min^{-1})	R^2
10	76.0	$4.5.10^{-3}$	0.993
15	57.9	$1.3.10^{-3}$	0.996
20	45.0	$1.2.10^{-3}$	0.951
25	36.0	$0.5.10^{-3}$	0.996

Table 2 presents a comparison of the photocatalytic degradation efficiency of CV on various photocatalytic materials. $NiFe_2O_4$ demonstrates a degradation efficiency of 76.0% under visible-light irradiation, significantly outperforming other materials, such as magnetic chitosan, ZrO_2-$CdZrO_3$, and graphene-$FeTiO_2$. For example, magnetic chitosan achieves a degradation efficiency of 72%; ZrO_2-$CdZrO_3$ under sunlight shows a degradation efficiency of 19%, and graphene-$FeTiO_2$ achieves only 14.3% under visible light. These findings are in agreement with those in recent studies, which have consistently shown that $NiFe_2O_4$ is one of the most efficient photocatalysts for organic dye degradation under visible-light conditions.

Table 2. Comparison of CV degradation capacity on various materials

Material	Light Source	Time (min)	*F* %	Ref.
Magnetic-Chitosan	Visible	140	72.0	[22]
ZrO_2-$CdZrO_3$	Sun	30	19.0	[26]
Graphene-$FeTiO_2$	Visible	50	14.3	[4]
$NiFe_2O_4$	160 W Osram bulb	120	76.0	This work

4 Conclusions

In this study, $NiFe_2O_4$ nanoparticles were successfully synthesised with a green approach, with starch as the reducing agent. The material was extensively characterised, and its photocatalytic performance was evaluated through the degradation of CV under visible light. The results indicate that $NiFe_2O_4$ exhibited a high degradation efficiency of 76.0% after 120 minutes, making it a highly effective photocatalyst for dye degradation. The photocatalytic process followed pseudo-first-order kinetics, with the rate constants calculated for different initial CV concentrations.

Furthermore, a comparison with other photocatalysts revealed that $NiFe_2O_4$ outperformed several materials, including magnetic chitosan and ZrO_2-$CdZrO_3$, in terms of degradation efficiency, thus highlighting its potential for environmental applications. The excellent photocatalytic performance of $NiFe_2O_4$ was attributed to its mesoporous structure, relatively large surface area, and the availability of active sites, which enhanced its reactivity under visible light. These findings were consistent with those in recent studies on $NiFe_2O_4$ and similar photocatalytic materials, confirming the effectiveness of $NiFe_2O_4$ for environmental remediation, particularly in the degradation of organic dyes. Future studies may focus on optimising the synthesis process, exploring the recyclability of $NiFe_2O_4$, and evaluating its performance in real wastewater treatment scenarios.

Acknowledgement

This research was funded by University of Medicine and Pharmacy, Hue University, under grant number 10/25.

Conflict of interest

The authors declare that there are no conflicts of interest regarding the publication of this paper.

pISSN 1859-1388
eISSN 2615-9678

References

1. Irshad Z, Bibi I, Ghafoor A, Majid F, Kamal S, Ezzine S, et al. Ni doped $SrFe_{12}O_{19}$ nanoparticles synthesised via micro-emulsion route and photocatalytic activity evaluation for the degradation of crystal violet under visible light irradiation. Results Phys. 2022;42:106006.
2. Komal, Srivastava RC, Joshi CS, Verma HK. Zinc oxide and nickel ferrite nanocomposite as an efficient photocatalyst for crystal violet dye degradation. Solid State Commun. 2024; 386:115517.
3. Ahmad W, Khan A, Ali N, Khan S, Uddin S, Malik S, et al. Photocatalytic degradation of crystal violet dye under sunlight by chitosan-encapsulated ternary metal selenide microspheres. Environ Sci Pollut Res. 2021;28(7):8074-87.
4. Shende TP, Bhanvase BA, Rathod AP, Pinjari D V, Sonawane SH. Sonochemical synthesis of Graphene-Ce-TiO_2 and Graphene-Fe-TiO_2 ternary hybrid photocatalyst nanocomposite and its application in degradation of crystal violet dye. Ultrason Sonochem. 2018;41:582-9.
5. Katubi KM, Aslam A, Khalil S, Alrowaili ZA, Al-Buriahi MS, Anwar M, et al. Synthesis and characterisation of graphitic carbon nitride composite with $NiFe_2O_4$/CdO for photocatalytic treatment of diclofenac sodium and crystal violet. Opt Mater (Amst). 2023;139:113721.
6. Farooq A, Alzahrani FMA, Alomayrah N, Manzoor A, Alrowaili ZA, Al-Buriahi MS, et al. Solar light driven enhanced photocatalytic efficiency of Graphene based composite of co-doped Bismuth Ferrite ($Ba_{0.5}$ $Bi_{0.5}$ $Nd_{0.5}$ $Fe_{1.5}$ O_3/$Gr_{0.375}$) for Crystal Violet and Paracetamol. Curr Appl Phys. 2024; 63:126-35.
7. Khan I, Saeed K, Zekker I, Zhang B, Hendi AH, Ahmad A, et al. Review on Methylene Blue: Its Properties, Uses, Toxicity and Photodegradation. Water. 2022;14(2):242.
8. Khalil LB, Rophael MW, Mourad WE. The removal of the toxic Hg(II) salts from water by photocatalysis. Appl Catal B Environ. 2002; 36(2):125-30.
9. Rao R, Zhang X, Sun X, Wang M, Ma Y. Effects of elemental chemical state in $NiFe_2O_4$@ TiO_2 on the photocatalytic performance. J Wuhan Univ Technol Sci Ed. 2020;35(2):320-6.
10. Jihad KM, Roknabadi MR, Mohammadi M, Goharshadi EK. Reduced graphene oxide/TiO_2/$NiFe_2O_4$ nanocomposite as a stable photocatalyst and strong antibacterial agent. Sustain Environ Res. 2023;33(1).
11. Zhao DF, Yang H, Li RS, Ma JY, Feng WJ. Fabrication of nickel ferrite–graphene nanocomposites and their photocatalytic properties. Mater Res Innov. 2014;18(7):519-23.
12. Zhang H, Xia B, Wang P, Wang Y, Li Z, Wang Y, et al. From waste to waste treatment: mesoporous magnetic $NiFe_2O_4$/ZnCuCr-layered double hydroxide composite for wastewater treatment. J Alloys Compd. 2020;819:153053.
13. Karunakaran G, Jagathambal M, Van Minh N, Kolesnikov E, Kuznetsov D. Green Synthesis of $NiFe_2O4$ Spinel-Structured Nanoparticles Using Hydrangea paniculata Flower Extract with Excellent Magnetic Property. JOM. 2018;70(7):1337-43.
14. Xiang W, Hernandez S, Hosseini P, Bai F, Hagemann U, Heidelmann M, et al. Unveiling Surface Species Formed on Ni-Fe Spinel Oxides During the Oxygen Evolution Reaction at the Atomic Scale. Adv Sci. 2025;2501967.
15. Adeleke JT, Theivasanthi T, Thiruppathi M, Swaminathan M, Akomolafe T, Alabi AB. Photocatalytic degradation of methylene blue by ZnO/$NiFe_2O_4$ nanoparticles. Appl Surf Sci. 2018;455:195-200.
16. Wang Y, Wang H, Yang Y, Xin B. Magnetic $NiFe_2O_4$ 3D nanosphere photocatalyst: Glycerol-assisted microwave solvothermal synthesis and photocatalytic activity under microwave electrodeless discharge lamp. Ceram Int. 2021; 47(10):14594-602.
17. Taqvi SIH, Solangi AR, Buledi JA, Khand NH, Junejo B, Memon AF, et al. Plant extract-based green fabrication of nickel ferrite ($NiFe_2O_4$) nanoparticles: An operative platform for non-enzymatic determination of pentachlorophenol. Chemosphere. 2022;294:133760.
18. Tong SK, Chi PW, Kung SH, Wei DH. Tuning bandgap and surface wettability of $NiFe_2O_4$ driven by phase transition. Sci Rep. 2018;8(1):1338.
19. Bhosale S V, Kanhe NS, Bhoraskar S V, Bhat SK, Bulakhe RN, Shim JJ, et al. Micro-structural analysis of $NiFe_2O_4$ nanoparticles synthesised by thermal plasma route and its suitability for BSA adsorption. J Mater Sci Mater Med. 2015;26:1-15.

20. Ashery A, Zawrah M, Abou Hammad AB, El-Okr MM, Zawrah MF, Abou Hammad AB. Structural and Magnetic Analysis on Spinel ($NiFe_2O_4$) Prepared By Sol Gel Process at Different Calcinations Temperatures. Artic IOSR J Appl Phys. 2016;8(3):15-9.

21. Moradi-Bieranvand M, Farhadi S, Zabardasti A, Mahmoudi F. Construction of magnetic MoS_2/$NiFe_2O_4$/MIL-101(Fe) hybrid nanostructures for separation of dyes and antibiotics from aqueous media. RSC Adv. 2024;14(16):11037-56.

22. Massoudinejad M, Rasoulzadeh H, Ghaderpoori M. Magnetic chitosan nanocomposite: fabrication, properties, and optimization for adsorptive removal of crystal violet from aqueous solutions. Carbohydr Polym. 2019;206:844-53.

23. Eisavi R, Ghadernejad S. $NiFe_2O_4$@SiO_2–Cu as a novel and efficient magnetically recoverable nanocatalyst for regioselective synthesis of β-thiol-1, 2, 3-triazoles under benign conditions. RSC Adv. 2023;13(40):27984-96.

24. Zahra S, Naz U, Irshad M, Sheikh A, Zahra S. Effect of calcination temperature on structural and magnetic properties of polypropylene glycol stabilised nickel ferrite nanoparticles. BMC Chem. 2025;19(1):106.

25. Kumar P V, Short MP, Yip S, Yildiz B, Grossman JC. High surface reactivity and water adsorption on $NiFe_2O_4$ (111) surfaces. J Phys Chem C. 2013; 117(11):5678-83.

26. Tavakoli-Azar T, Mahjoub A, Sadjadi MS, Ghaznavi-Ghoushchi MB. Enhanced photocatalytic activity of ZrO_2-$CdZrO_3$-S nanocomposites for degradation of Crystal Violet dye under sunlight. J Photochem Photobiol A Chem. 2022;426:113746.